

# Coupled measurements of hydraulic permeability and full stiffness tensor compaction trends in artificial shales

**Roman Beloborodov\***  
CSIRO Energy  
Perth  
BeloborodovRM@gmail.com

**Marina Pervukhina**  
CSIRO Energy  
Perth  
Marina.Pervukhina@csiro.au

**Maxim Lebedev**  
Curtin University  
Perth  
M.Lebedev@curtin.edu.au

*\*presenting author asterisked*

## SUMMARY

Understanding of compaction trends of elastic and hydraulic properties in anisotropic shales is crucial for exploration of energy resources, ecological disposal of nuclear waste, and hydrogeological applications. However, complexity of the natural shale mineralogy and lack of quality data available for analysis results in poor knowledge of these compaction trends.

Careful control over the shale mineralogy, pore fluid composition and applied stresses allows us to simulate the natural environments and acquire quality data on the properties of artificial shales. Here for the first time we present methodology and describe a setup that allows simultaneous acquisition of all five independent elastic constants and extremely low hydraulic permeability values of transversely isotropic artificial shale samples during mechanical compaction experiments (porosity decrease from 40% to 10%).

Hydraulic permeabilities of artificially compacted samples are comparable to the ones of natural shales. Permeability drops exponentially with compaction. Silt fraction and clay mineralogy are the two key parameters that are responsible for broad variations of permeability in shales with the same porosity. We provide analytical equations that allow calculating permeability if porosity and silt fraction are known.

Elastic constants of clay matrix exhibit positive linear trends with the porosity decrease. Small variations in clay mineralogy have a minor effect on absolute values of elastic coefficients or anisotropy but lead to noticeable increase of the compressional ( $V_P$ ) to shear ( $V_S$ ) velocities ratio at the same porosity. Finally, strong correlations ( $R^2$  above 0.95) of the hydraulic permeability with acoustic impedance and  $V_P/V_S$  ratio are observed for all the prepared samples.

**Key words:** Compaction trends, permeability, elastic anisotropy, shale.

## INTRODUCTION

Knowledge of the fluid permeability of mudstones is crucial for hydrogeology, basin modelling and nuclear waste disposal (Hasanov 2014, Wang, et al. 2013). Although mudstones (including shales) comprise 70 % of sedimentary basins and serve as seals in conventional reservoirs or play a role of unconventional reservoir themselves, the link between measurable parameters and the hydraulic permeability is still poorly understood (Dewhurst, et al. 1998). This can be attributable to a limited number of permeability measurements on mudstones due to (1) the challenge to measure the extremely low permeabilities that are specific to shales and large experimental errors associated with these measurements, and (2) the fact that shale intervals are rarely cored. However, even the limited sampling pool and errors cannot explain the fact that permeabilities are of three orders in magnitude different for mudstones with the same porosity (Yang and Aplin 2010).

The anisotropic elastic properties of clay rocks and their compaction trends are of crucial practical importance for seismic imaging, time to depth conversion and correct seismic interpretation. Elastic properties and their anisotropy of both natural and artificial shales were shown to be strongly affected by rock mineralogy and microstructure (e.g. Bandyopadhyay 2009, Beloborodov, et al. 2016, Dewhurst and Siggins 2006, Lonardelli, et al. 2007). To avoid uncertainties and inhomogeneity that are also associated with natural samples and resedimented clays, experimental studies were conducted on artificial mudstone samples with controlled clay mineralogy and characterized with distinct vertical transverse isotropy (VTI) (Beloborodov, et al. 2016, Zadeh, et al. 2016). However, most of the studies were limited to vertical velocities (normal to bedding) of such artificially compacted samples (e.g. Fawad, et al. 2010, Mondol, et al. 2008, Zadeh, et al. 2016). Beloborodov et al. (2016) described an experimental rig that allowed measuring P-wave velocities normal and parallel to bedding and S-wave velocity propagating normal to bedding.

We present a methodology that allows simultaneous acquisition of the five independent elastic constants of a transversely isotropic shale sample and its fluid permeability during compaction experiments. These unique simultaneous measurements allow obtaining the compaction trends of fluid permeability and elastic properties as well as the correlations of vertical (normal to bedding) permeability with such seismic attributes as  $V_P/V_S$  ratio and acoustic impedance calculated from vertical velocities. We present the results for three quartz-kaolinite samples and two quartz-smectite-kaolinite samples.

## METHODOLOGY

### Experimental setup

The compaction setup used in our experiments is shown in Figure 1. The oedometer cell and pistons that conduct pressure to the sample are made of polyether ether ketone (PEEK) plastics. Constant axial stress is applied vertically on the top piston by the hydraulic actuator connected to the automatic syringe pump (Isco-Teledyne 260D).

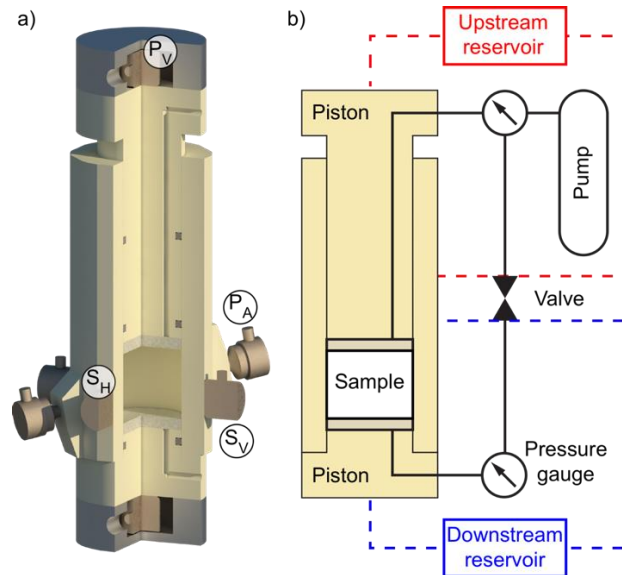


**Figure 1. Schematics of the experimental compaction setup. a) 3D-section of the compaction oedometer cell illustrating the positioning of piezoelectric ultrasonic transducers:  $P_V$ ,  $P_A$  – for measuring the vertical and angular P-wave velocities,  $S_V$ ,  $S_H$  – for measuring slow and fast S-wave velocities, respectively, and also the horizontal P-wave velocity. b) Principle scheme of the hydraulic system for permeability measurements via pressure-oscillation technique.**

The setup allows conducting the experiment in an undrained and drained compaction regime. The space between the cell and the pistons is sealed with silicone rings to prevent the leakage of connate water. Both pistons have through drainage channels connected to the automatic pump via the high-pressure pipelines that allow accurate control of the pore pressure and fluid flow within the sample (Figure 1b). Pore pressure at the top and bottom reservoirs can be monitored and controlled independently via the two pressure gauges installed on either side of the separating valve.

Four pairs of high-frequency ultrasonic piezoelectric transducers, attached to the cell and pistons (Figure 1a), allow measuring the propagation times of ultrasonic pulses travelling within the sample in three directions. Thus, two pairs of S-wave transducers (central frequency of 1 MHz) are attached to the walls of the cell in horizontal plane. One pair is polarized along the axis of cell symmetry ( $S_V$ ) while the other one is polarized normal to it ( $S_H$ ). A pair of P-wave transducers ( $P_A$ ) (central frequency 2.5 MHz) is positioned at the angle of  $80^\circ$  from the cell symmetry axis. The last pair of P-wave transducers ( $P_V$ ) (central frequency 1 MHz) is attached to the top and the bottom plastic pistons. This combination allows estimation of the P-wave velocities ( $V_p$ ) in the vertical and horizontal directions, and at an arbitrary angle to the sample's symmetry axis along with the both slow and fast S-wave velocities ( $V_s$ ). Assuming the vertical polar anisotropy of the sample, based on our previous results obtained with neutron diffraction goniometry (Beloborodov, et al. 2016), full tensor of elasticity can be calculated from the measured data at any stage of the compaction process.

### Preparation of samples

Following the procedure described in Beloborodov, et al. (2016), five mixtures are prepared for compaction experiments. Three samples are kaolinite based mixtures with 0, 20 and 40 weight percent of quartz inclusions. Two mixed-clay samples (1:9 smectite-kaolinite weight ratio) are made with 0 and 20 weight percent of quartz. The quartz powder consists of silt-sized grains (38–56  $\mu\text{m}$ ) with mean aspect ratio of 0.5 (oblate spheroids). Kaolinite and smectite powders are in aggregated state, i.e. in a form of large associations ( $\leq 70 \mu\text{m}$ ) of aligned individual clay particles ( $\leq 2 \mu\text{m}$ ).

### Compaction procedure and velocity measurements

Compaction is implemented by steps, where each step consists of three stages: 1) drained consolidation of the sample under the constant axial stress, 2) application of the pore pressure equal to the appropriate hydrostatic one, 3) release of the applied pore pressure. Permeability measurements take place at the second stage of each compaction step when there is no flux from and out of the reservoirs connected to the sample. The travel times of acoustic waves are measured at each stage of compaction steps. Phase velocities of P- and S-waves are easily evaluated for horizontal and vertical directions by dividing the chosen dimension of a sample by the calculated time of wave propagation within the sample in that direction. In our experiments, the phase velocity at an angle to the sample's symmetry

axis cannot be measured directly, as the distance between transducers is significantly larger than their diameter (see Dellinger and Vernik 1994), but instead it is calculated from the measured group velocity as suggested by Miller, et al. (2012).

### Permeability measurements

For permeability measurements, we use pressure-oscillation technique that is comprehensively described in the works of Bernabé, et al. (2006), Fischer (1992), Kranz, et al. (1990), Song and Renner (2007) and summarized by Hasanov (2014). Schematics of the experimental setup for permeability measurements is shown in Figure 1b. A sample inside the oedometer is connected to the upstream and downstream reservoirs at its top and bottom faces respectively. The volumes of upstream and downstream reservoirs are 260 and 2.5 cm<sup>3</sup> respectively. The volume of the sample's pore space during compaction changes from ~15 to ~5 cm<sup>3</sup>. Prior to the experiment reservoirs are connected through the valve between them; this allows equilibrating the initial pore pressure within the sample and both reservoirs. After the equilibrium is reached the valve is closed to ensure the independent monitoring of input and output pressure changes in upstream and downstream reservoirs, respectively. The harmonic pressure oscillations  $P_U = A_U e^{i(\omega t)}$  are initiated at the upstream reservoir with the programmable pump so that amplitude of oscillation does not exceed 10 % of the initial pore pressure created within the system at a given compaction stage and the period is set to be sufficient for registering the pressure oscillation at the downstream reservoir  $P_D = A_D e^{i(\omega t + \theta)}$ . Further hydraulic properties of a sample are calculated from the amplitude ratio ( $A_r = A_U/A_D$ ) and phase lag ( $\theta$ ) between the pressure oscillations in upstream and downstream reservoirs.

The analytical solution for the pressure diffusion equation is given by Bernabé, et al. (2006) in the following form:

$$A_r e^{-i\theta} = \left( \cosh \left[ \sqrt{\frac{\xi}{\eta}} (1+i) \right] + \frac{1+i}{\sqrt{\xi\eta}} \sinh \left[ \sqrt{\frac{\xi}{\eta}} (1+i) \right] \right)^{-1}, \quad (1)$$

where  $A_r$  and  $\theta$  are the experimentally obtained amplitude ratio and phase lag, respectively. The dimensionless parameters: storage capacity  $\xi$  and permeability  $\eta$  in Eq. 1 are defined by

$$\xi = \frac{AL\beta_{st}}{\beta_d}, \eta = \frac{2Ak}{\omega L\mu\beta_d}, \quad (2)$$

where  $A$  is the sample cross-section area,  $L$  the sample length,  $\beta_{st}$  the sample storativity,  $\beta_d$  the downstream reservoir storage,  $k$  the sample permeability and  $\mu$  the dynamic viscosity of the pore fluid.

Bernabé, et al. (2006) noticed that if the dimensionless parameter  $\xi$  approaches zero, Equation 1 converges to the following form

$$\eta = \frac{2A_r}{\sqrt{1 - A_r^2}}, \quad (3)$$

i.e., permeability can be deduced from amplitude ratio  $A_r$  alone. We use Equations 2, 3 to estimate the permeability of the samples, as in our case the dimensionless storativity  $\xi$  approaches 0 due to the insignificant difference between the storage capacity of a sample and the downstream reservoir and the small sample size.

## RESULTS

### Elastic properties

Five independent elastic constants and Thomsen's anisotropy parameters  $\varepsilon$ ,  $\gamma$ , and  $\delta$  (Thomsen 1986) are calculated from the measured velocities and densities for the five artificial shale samples (Figure 2). All the elastic constants exhibit almost linear increase with porosity reduction from 0.40 to 0.15. Moduli  $C_{11}$  and  $C_{66}$  that correspond to the P- and horizontally polarized S-wave velocities measured in horizontal direction noticeably exceed  $C_{33}$ ,  $C_{44}$ , calculated from velocities measured in vertical direction. P-wave anisotropy parameter  $\varepsilon$  increases almost linearly with porosity reduction. In contrast, the S-wave anisotropy parameter  $\gamma$  initially characterized with significant values of 0.5-0.7 decreases with compaction. The anisotropy parameter  $\delta$  fluctuates around some constant value so that  $\delta < |0.2|$ . The increase of quartz content leads to the substantial decrease in absolute values of the anisotropy parameters via stiffening of the clay matrix in direction normal to the bedding and weakening of the clay particle orientation. This effect may be observed in both kaolinite-based samples (Figure 2a, b, c) and mixed-clay-based samples (Figure 2d, e).

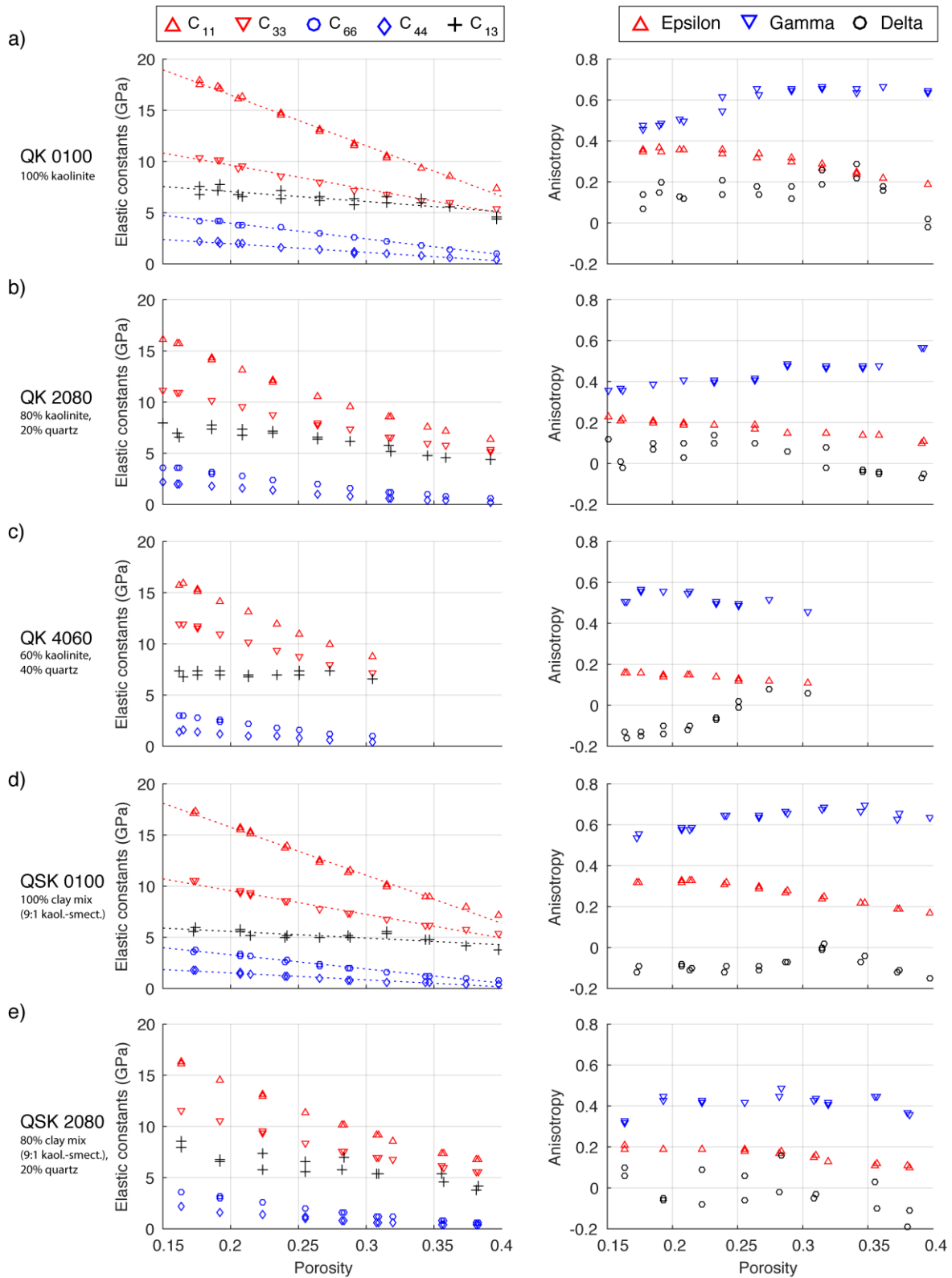


**Figure 2. Elastic constants (left hand side) and Thomsen's anisotropy parameters  $\epsilon, \gamma, \delta$  (right hand side) versus porosity for the five artificial shale samples. Dashed lines show best linear fit for the elastic constants of the pure clay samples.**

### Permeability

Variations of permeability with porosity in the direction perpendicular to bedding plane obtained for the five samples are shown in Figure 3 in semi-logarithmic scale. Permeability decays exponentially by an order of magnitude in all the samples during the compaction. In the pure kaolinite sample, permeability drops from  $10^{-19}$  to  $2 \cdot 10^{-20}$  m<sup>2</sup> while porosity decreases from 0.40 to 0.18. The pure clay kaolinite-smectite sample shows lower permeability values that decrease from  $4 \cdot 10^{-20}$  to  $9 \cdot 10^{-21}$  m<sup>2</sup> on a porosity range of

0.35–0.17. The increase of quartz content by 20 wt% results in the increase of permeability by approximately half an order of magnitude in both the kaolinite and mixed-clay based samples.

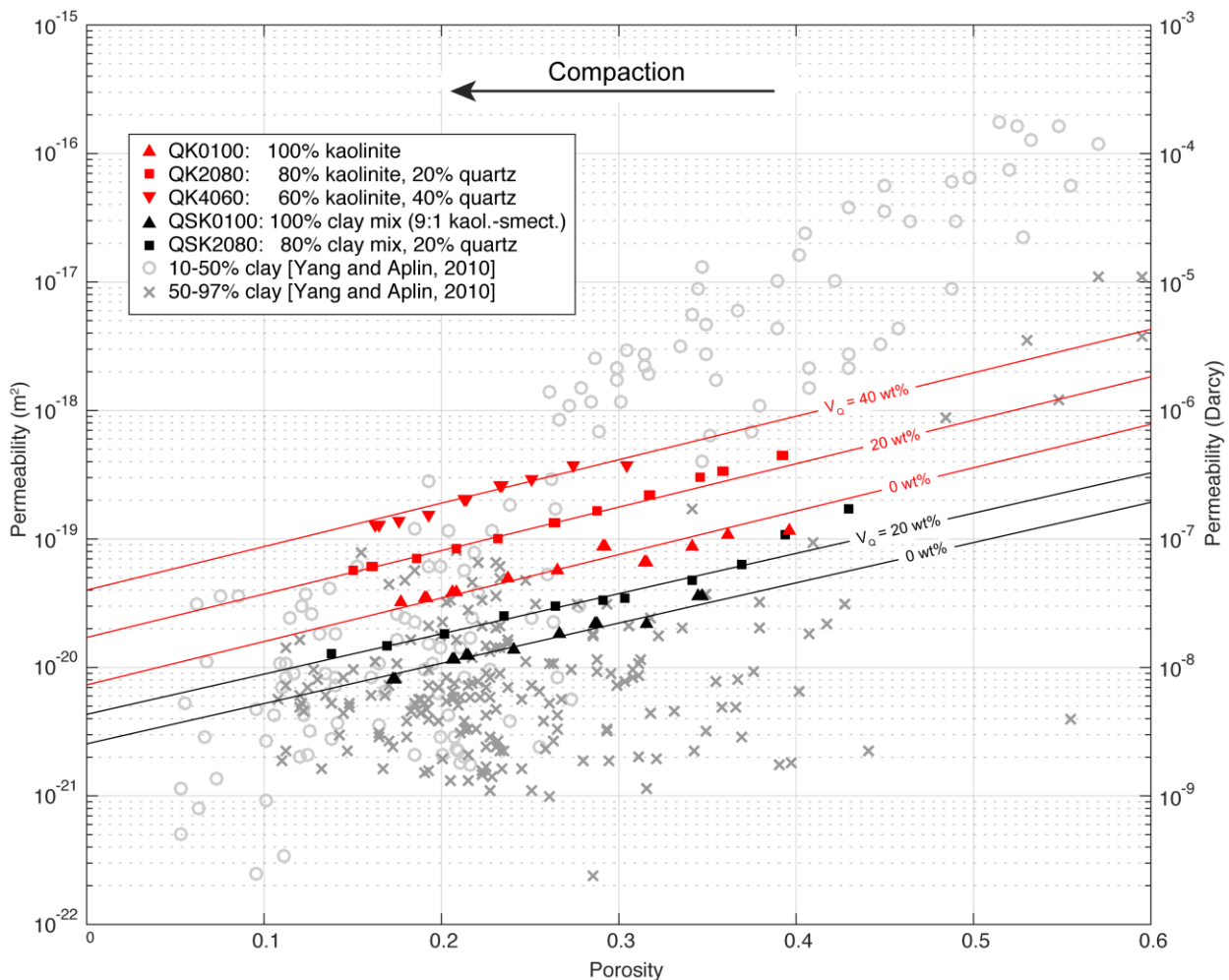


**Figure 3. Hydraulic permeability compaction trends in the artificial shale samples in comparison with Yang and Aplin (2010) data on permeability-porosity relationships in natural mudstones and shales. Solid lines show multiple linear regression fit calculated for given values of quartz content and porosity values.**

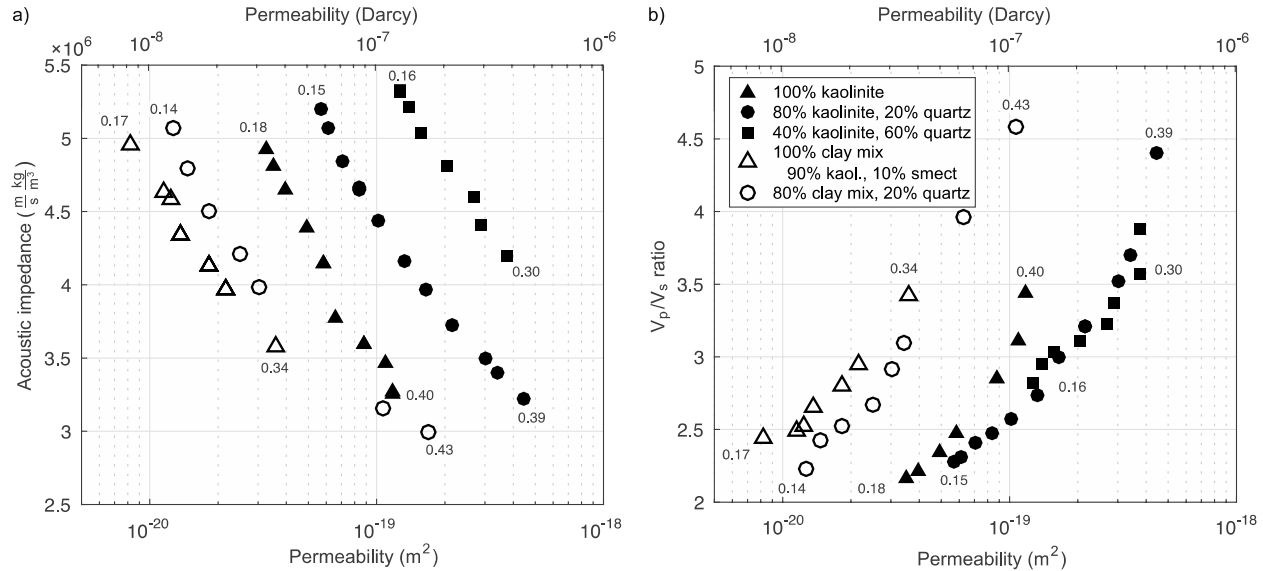
Higher permeability of the quartz-bearing samples might result from additional porosity formed on quartz-kaolinite interfaces (Keller, et al. 2011) and this porosity may have a dominating effect on their bulk permeability. At the same porosity level, the alignment of clay aggregates is weaker in the samples containing quartz (Beloborodov, et al. 2016) that assures the lower tortuosity of their pore network in the direction normal to the bedding. Similarly, the wet clay porosity (i.e. porosity of the clay matrix) is also higher that implies larger pore throats within the pore network.

Figure 3 allows comparing our results with experimentally obtained and modelled porosity-permeability relations for natural argillaceous rocks and shallow marine sediments (Yang and Aplin 2010). Although the permeabilities measured on the quartz-kaolinite artificial shales lay within the permeability-porosity range of natural rocks, they overestimate the permeability of the natural mudstones with high clay content (50–97 %). This fact can be explained with the mineralogy difference between the kaolinite based artificial shales and natural shales as the latter almost always contain some amount of smectite clay minerals that strongly reduce the permeability due to their swelling nature, small size of the particles, and vast specific surface area of  $\sim 800 \text{ m}^2/\text{g}$  compared to  $\sim 40 \text{ m}^2/\text{g}$  of kaolinite. As implied by the Kozeny-Carman equation, permeability is inversely proportional to the square of the specific surface area which means that the presence of even small amount of smectite clay minerals can significantly reduce the permeability of a mudstone. Here we show that additional 10 % of smectite in pure clay sample reduces the permeability by half an order of magnitude compared to pure kaolinite sample at the same porosity. Moreover, some deeply buried natural shales could have undergone a high-temperature chemical compaction that initiates formation of autogenic minerals into a pore space, the process that further reduces their permeability. Thus, low porosity in natural shales could be attributed to chemical alterations of shale constituents, while artificial samples in our experiments are subjected to pure mechanical compaction.

#### Elastic-hydraulic coupling

The hydraulic and elastic properties of the artificial shales, for the first time acquired simultaneously during the laboratory mechanical compaction, allow us to investigate the correlations between these properties. Figure 4 illustrates the variation of acoustic impedance

( $AI$ ), calculated from the density and vertical compressional P-wave as follows  $AI = \rho V_p$ , and the ratio of compressional and shear velocities normal to bedding ( $V_p/V_s$ ) versus permeability. Strong correlations ( $R^2 > 0.95$ ) of  $AI$  and  $V_p/V_s$  ratios with logarithm of hydraulic permeability are observed for all the samples. At the same  $AI$ , an increase of quartz fraction shifts the permeability compaction trend to higher permeabilities, while the increase in smectite content results in lower permeabilities. In turn  $V_p/V_s$  vs permeability plot clearly separates the samples with different composition of clay fraction, whereas variations in quartz content show no significant separation.



**Figure 4. Coupling of seismic parameters and hydraulic permeability for the compacted samples: a) Acoustic impedance vs permeability and b)  $V_p/V_s$  ratio vs permeability. Initial and final porosities are shown by numbers at the endpoints of each sample.**

## CONCLUSIONS

The newly developed experimental rig, with which all five independent elastic coefficients of TI medium can be measured, enables better understanding of the elastic anisotropy in shales and its evolution during mechanical compaction. Pressure-oscillation technique has been used for acquisition of the permeability compaction trends in shales. These simultaneous measurements provide comprehensive information on poorly understood compaction trends of anisotropic elastic properties and permeability in shales.

Hydraulic permeabilities of artificially compacted shale samples are comparable to these of natural analogs. Permeability drops exponentially with compaction. Silt fraction and clay mineralogy are the two key parameters that might be responsible for broad variations of permeability in clay rocks with the same porosity. We show the feasibility and provide examples of obtaining the empirical equations for calculating the permeability if porosity and silt fraction are known.

Elastic coefficients of clay matrix exhibit positive linear trends with the porosity decrease. The presence of 10 % of smectite in clay matrix has a minor effect on absolute values of elastic coefficients or anisotropy but leads to noticeable increase in the ratio of compressional to shear velocity ( $V_p/V_s$ ) normal to bedding at the same porosity. Finally, strong correlations ( $R^2$  above 0.95) of the hydraulic permeability with acoustic impedance and  $V_p/V_s$  ratio are observed for all the prepared samples. These results illustrate that the permeability of shales is impossible to predict from seismic data alone without a prior knowledge on their mineral composition.

## ACKNOWLEDGMENTS

This work was funded through the CSIRO SHARPP project sponsored by Total. RB and ML would like to acknowledge ASEG Research Foundation for sponsoring them with Grant (RF16P05). RB was supported by Curtin Strategic International Postgraduate Research Scholarship and Australian Government Research Training Program Scholarship.

## REFERENCES

- Bandyopadhyay, K., 2009, *Seismic Anisotropy: Geological Causes and Its Implications to Reservoir Geophysics*. Stanford University.
- Beloborodov, R., Pervukhina, M., Luzin, V., Delle Piane, C., Clennell, M.B., Zandi, S., and Lebedev, M., 2016, Compaction of Quartz-Kaolinite Mixtures: The Influence of the Pore Fluid Composition on the Development of Their Microstructure and Elastic Anisotropy. *Marine and Petroleum Geology* **78**, 426-38.
- Bernabé, Y., Mok, U., and Evans, B., 2006, A Note on the Oscillating Flow Method for Measuring Rock Permeability. *International Journal of Rock Mechanics and Mining Sciences* **43**, 311-16.
- Dellinger, J. and Vernik, L., 1994, Do Travel-Times in Pulse-Transmission Experiments Yield Anisotropic Group or Phase Velocities. *Geophysics* **59**, 1774-79.
- Dewhurst, D.N., Aplin, A.C., Sarda, J.P., and Yang, Y.L., 1998, Compaction-Driven Evolution of Porosity and Permeability in Natural Mudstones: An Experimental Study. *Journal of Geophysical Research-Solid Earth* **103**, 651-61.
- Dewhurst, D.N. and Siggins, A.F., 2006, Impact of Fabric, Microcracks and Stress Field on Shale Anisotropy. *Geophysical Journal International* **165**, 135-48.
- Fawad, M., Mondol, N.H., Jähren, J., and Bjorlykke, K., 2010, Microfabric and Rock Properties of Experimentally Compressed Silt-Clay Mixtures. *Marine and Petroleum Geology* **27**, 1698-712.
- Fischer, G.J., 1992, Chapter 8 the Determination of Permeability and Storage Capacity: Pore Pressure Oscillation Method. in Evans Brian and Wong Teng-fong (eds.) *International Geophysics*, Academic Press, 187-211.
- Hasanov, A.K., 2014, Reservoir Transport and Poroelastic Properties from Oscillating Pore Pressure Experiments.
- Keller, L.M., Holzer, L., Wepf, R., Gasser, P., Munch, B., and Marschall, P., 2011, On the Application of Focused Ion Beam Nanotomography in Characterizing the 3d Pore Space Geometry of Opalinus Clay. *Physics and Chemistry of the Earth* **36**, 1539-44.
- Kranz, R.L., Saltzman, J.S., and Blacic, J.D., 1990, Hydraulic Diffusivity Measurements on Laboratory Rock Samples Using an Oscillating Pore Pressure Method. *International Journal of Rock Mechanics and Mining Sciences & Geomechanics Abstracts* **27**, 345-52.
- Lonardelli, I., Wenk, H.R., and Ren, Y., 2007, Preferred Orientation and Elastic Anisotropy in Shales. *Geophysics* **72**, D33-D40.
- Miller, D.E., Horne, S.A., and Walsh, J., 2012, Precise Inversion of Logged Slownesses for Elastic Parameters in a Gas Shale Formation. *Geophysics* **77**, B197-B206.
- Mondol, N.H., Bjorlykke, K., and Jähren, J., 2008, Experimental Compaction of Clays: Relationship between Permeability and Petrophysical Properties in Mudstones. *Petroleum Geoscience* **14**, 319-37.
- Song, I. and Renner, J., 2007, Analysis of Oscillatory Fluid Flow through Rock Samples. *Geophysical Journal International* **170**, 195-204.
- Thomsen, L., 1986, Weak Elastic-Anisotropy. *Geophysics* **51**, 1954-66.
- Wang, Q., Cui, Y.J., Tang, A.M., Barnichon, J.D., Saba, S., and Ye, W.M., 2013, Hydraulic Conductivity and Microstructure Changes of Compacted Bentonite/Sand Mixture During Hydration. *Engineering Geology* **164**, 67-76.
- Yang, Y.L. and Aplin, A.C., 2010, A Permeability-Porosity Relationship for Mudstones. *Marine and Petroleum Geology* **27**, 1692-97.
- Zadeh, M.K., Mondol, N.H., and Jähren, J., 2016, Experimental Mechanical Compaction of Sands and Sand-Clay Mixtures: A Study to Investigate Evolution of Rock Properties with Full Control on Mineralogy and Rock Texture. *Geophysical Prospecting* **64**, 915-41.